Materials Science and Engineering A 539 (2012) 93–100

Contents lists available at SciVerse ScienceDirect

Materials Science and Engineering A

journal homepage: www.elsevier.com/locate/msea

Influence of microstructure and its evolution on the mechanical behavior of modified MAR-M247 fine-grain superalloys at 871 °C

Jian-Hong Liao[a,*], Hui-Yun Bor[a], Chao-Nan Wei[a], Chuen-Guang Chao[b], Tzeng-Feng Liu[b]

[a] Materials and Electro-Optics Research Division, Chung-Shan Institute of Science and Technology, Taoyuan 32599, Taiwan, ROC
[b] Department of Materials Science and Engineering, National Chiao Tung University, Hsinchu 30049, Taiwan, ROC

ARTICLE INFO

Article history:
Received 3 May 2011
Received in revised form 3 December 2011
Accepted 11 January 2012
Available online 24 January 2012

Keywords:
Fine-grain
Nickel based superalloys
Casting
Rhenium
Creep

ABSTRACT

This study added Re to Mar-M247 fine-grain superalloy and investigated the influence of microstructure and its evolution on the mechanical behavior at 871 °C. Mar-M247 and modified Mar-M247 alloys consisted of dual precipitation of primary and secondary γ′ particles in the γ matrix. An increase in Re content led to a reduction in the primary γ′ phase with the γ′ phase becoming finer; however, the addition of Re did not have an obvious influence the secondary γ′ phase. Tensile and creep tests (871 °C/379 MPa) showed that both tensile and creep strength increased with an increase in Re content up to a maximum of 3 wt%. In the early creep stage, the addition of Re improved creep resistance by increasing the strength of the γ matrix and decreasing the inter-particle spacing. In the later creep stage, the linear fraction of the γ′ raft in stress axial direction increased following the addition of Re, resulting in improved creep resistance. Observation of microstructure evolution indicated that only secondary γ′ phase coarsened directionally into a rafting structure and the primary γ′ phase was unaffected by creep. An interrupted creep tests verified that the γ′ rafting structure initiated in the primary creep stage and completed in the secondary creep stage. The addition of excessive quantities of Re, such as 5 wt%, resulted in the formation of needle-like P phase, which damaged the tensile and creep properties. During tensile and creep tests, cracks initiated and propagated along grain boundary (GB) in alloys containing 0–3 wt% Re; and propagated along both the GB and P/γ interface in an alloy containing 5 wt% Re. In conclusion, optimal results were obtained for fine-grain Mar-M247 following the addition of 3 wt% Re.

1. Introduction

The fine-grain microstructure of Ni-base superalloys provides advantages, such as refined grain, carbides, and precipitates. The fine-grain process was developed to improve the strength, creep and fatigue life of disc rotors, turbine blades, and integral wheels working at intermediate temperatures (427–760 °C) [1–3]. However, for higher-temperature performance, such as turbine blades, a coarser grain microstructure would be preferred [1]. In fact, the desired grain size for integral casting is difficult to achieve, which has limited the wide scale application of fine-grain superalloy casting. To overcome this issue, engineers are seeking to develop new superalloys capable of maintaining high-temperature strength in fine-grain casting. Due to superior alloy design and control of the microstructure of Mar-M247, the fine-grain casting of this material has been applied at temperatures of up to 982 °C [4]. Therefore, this study proposes a modified alloy based on Mar-M247 to maintain high-temperature strength in fine-grain casting.

Basically, Mar-M247 is a high volume fraction γ′ alloy comprising approximately 60% volume fraction of ordered $L1_2$ γ′ precipitates in a disordered face-centered cubic γ matrix [5]. This alloy has been widely employed in the fabrication of advanced turbine blades and rotating parts in the aerospace industry because of its excellent castability and high-temperature properties [4,5]. Recently developed single-crystal superalloys contain high quantities of Re, which act as solid solution strengtheners to further improve the high-temperature capability [6,7]. Strengthening the solid solution of the γ matrix is one possible solution to further improve the strength of Mar-M247.

In this study, we selected Re as the element to modify Mar-M247; however, the introduction of this element leaves the microstructure susceptible to the formation of deleterious topologically closed packed (TCP) phases when exposed to elevated temperatures [6–9]. Therefore, the addition of Re must be strictly controlled in the design of superalloys to prevent formation of TCP phase.

Most studies to date have focused on the behavior of single crystal superalloys containing Re at high-temperatures and little research has addressed the influence of Re in fine-grain Ni-base superalloys. This study investigated fine-grain Mar-M247 using

* Corresponding author. Tel.: +886 3 4712201x357254; fax: +886 3 4111334.
E-mail address: stanley.liaw@msa.hinet.net (J.-H. Liao).

0921-5093/$ – see front matter © 2012 Elsevier B.V. All rights reserved.
doi:10.1016/j.msea.2012.01.059

Table 1
The chemical compositions of superalloys investigated (wt%).

Alloy	Re	Cr	Co	Mo	W	Ta	Al	Ti	Hf	C	B	Zr	Ni
Mar-M247	–	8.35	10.10	0.69	9.91	3.05	5.42	1.00	1.32	0.15	0.02	0.04	bal.
A(1Re)	0.97	8.41	9.98	0.69	10.02	2.99	5.38	0.98	1.22	0.14	0.02	0.04	bal.
B(3Re)	2.92	8.42	9.99	0.69	10.02	3.01	5.33	0.98	1.29	0.14	0.02	0.04	bal.
C(5Re)	4.99	8.40	10.00	0.70	10.03	2.99	5.37	0.97	1.22	0.14	0.02	0.04	bal.

various quantities of Re, from 0 to 5 wt%, focusing on microstructure and its evolution on the mechanical behavior at 871 °C, to determine the optimal proportion of added Re.

2. Experimental

In this study, 0, 1, 3, and 5 wt% Re were added to Mar-M247 superalloy and named as Mar-M247, A(1Re), B(3Re), and C(5Re), respectively. The nominal chemical compositions of the alloys investigated are listed in Table 1. Each of the alloys was melted in a vacuum furnace and poured into an investment mold using the Microcast-X technique to obtain cast rods. Microcast-X is the second generation of fine-grain casting technique developed by Howmet Corporation, with controlled low pouring temperature and a high heat-extraction rate to limit the growth of grains [2,3,10,11]. The pour and mold temperatures were 1380 and 1100 °C, respectively. The chemistry of each alloy was determined using X-ray fluorescence, with the exception of the Re content, which was determined by inductive coupled plasma chemical analysis. Hot-isostatic press (HIP) and heat treatment conditions were conducted according to fine-grain specification in Refs. [4,5]. HIP was utilized in this study to avoid casting pores that would affect the results of tensile and creep tests. The HIP parameters were 1185 °C under argon at a pressure of 172.4 MPa for 4 h, followed by cooling in argon gas. Heat treatment of the solid solution was conducted at 1185 °C for 2 h in vacuum, followed by cooling in argon gas. Samples were subjected to aging heat treatment at 871 °C for 20 h in a vacuum followed by cooling to room temperature (RT) in a furnace.

General metallographic samples were polished and etched using 10 ml HNO_3 + 5 ml HCl + 30 ml lactic acid. Grain size was measured by determining the mean linear intercept of the grains using optical microscope (OM). A scanning electron microscope (SEM) equipped with energy dispersive spectroscope (EDS) was used to characterize the microstructure. SEM images were obtained using the secondary electron mode at 20 kV. Quantitative statistical analysis of the γ′ phase was performed on a large number of SEM photos at various magnifications using an image analyzer. Transmission electron microscope (TEM) operated at 200 kV to determine the crystal structure of the TCP phase. TEM thin foils were prepared by twin-jet thinning electrolytically in a solution of 90% CH_3COOH + 10% $HClO_4$.

Tensile tests were performed using an Instron 1125 universal test machine with 0.2 mm/min. crosshead speed at RT, 760 °C, and 871 °C in atmosphere. Constant load creep tests were performed at 871 °C/379 MPa in air using SATEC M3 creep testers. Test bars with a gage diameter of 6.3 mm and length of 32 mm were machined from the heat-treated cast rods. At least four tensile and creep tests were conducted under each test condition. Fracture surfaces were characterized by SEM. Longitudinal sections were metallographically prepared, as described above, and examined using SEM.

3. Results

3.1. Microstructures

Generally, Microcast-X provides the ability to produce castings with a grain size of 65–125 μm [3,10]. Fig. 1a shows an OM image of Mar-M247, in which the grain size is clearly consistent with Microcast-X casting, as previously described. The grain size of other alloys is similar to that of Mar-M247. Fig. 1b shows that the microstructure of the Mar-M247 comprised γ matrix, γ′ particles, rosette-like γ–γ′ eutectic, and carbides. Basically, the microstructures of A(1Re) and B(3Re) were similar to that of Mar-M247. Fig. 2a shows the microstructure of C(5Re), and the obvious difference is the needle-like precipitates (TCP phases) 10–20 μm long within the grain interior, compared to Mar-M247. EDS measurements indicated that TCP phases had high proportions of Re, W, Cr, and Co (Fig. 2b). The crystal structure of the TCP phases varies considerably. For instance, the μ and R phases are rhombohedral, the P phase is orthorhombic, and the σ phase is tetragonal [6,7]. According to TEM analysis (Fig. 3), the TCP in C(5Re) is identified as P phase, with an orthorhombic structure and lattice constant a = 0.901 nm, b = 1.689 nm, and c = 0.471 nm. Fig. 4 shows a highly magnified SEM image of the morphology of γ′ precipitates and Table 2 summarizes the quantitative statistical results. Mar-M247 consists of dual size of γ′ precipitate. Primary γ′ phases with block morphology are 1450 nm in average size, occupying 43% of the area fraction. Secondary γ′ phases with an average size of 85 nm occupied 19% of the area fraction. No primary γ′ in cuboidal was observed in the

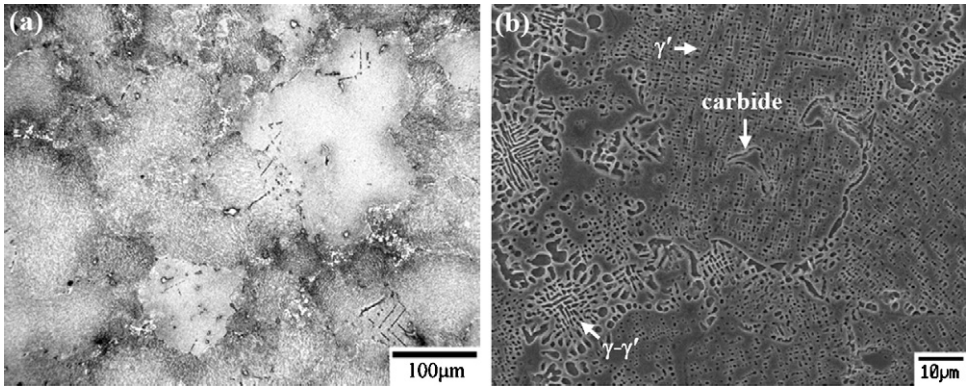

Fig. 1. The microstructure of original Mar-M247 after heat treatment: (a) OM and (b) SEM.

Table 2
Summary of the characteristics of γ′ (Af: area fraction; σ: standard deviation).

Alloy	Primary γ′		Secondary γ′		Inter-particle spacing[*1]	Width of γ channel[*2]
	Af (%)	Size ± σ (nm)	Af (%)	Size ± σ (nm)	Spacing ± σ (nm)	Width ± σ (nm)
Mar-M247	43	1450 ± 510	19	85 ± 20	2080 ± 650	640 ± 180
A(1Re)	42	1410 ± 500	19	83 ± 19	2010 ± 625	635 ± 175
B(3Re)	38	325 ± 105	20	74 ± 22	805 ± 245	470 ± 160
C(5Re)	26	260 ± 60	20	70 ± 20	1020 ± 435	710 ± 310

[*1] The inter-particle spacing is defined as the distance between the centers of the neighboring primary γ′ particles.
[*2] The width of γ channel is defined as the distance between the edges of the neighboring primary γ′ particles.

alloy without Re addition. With an increase in Re content, the primary γ′ phase becomes increasingly fine and cuboidal, and its area fraction decreased. The size of secondary γ′ slightly decreased with an increase in Re; however, the area fraction of secondary γ′ was nearly invariable. The total area fraction of γ′ phase decreased as the Re content increased. In addition, the inter-particle spacing and the width of the γ channel decrease with Re content up to a minimum of 3 wt%.

Finally, it should be emphasized that no casting pores were observed in any of the alloys, ensuring that the tensile and creep test results were not influenced by casting pores.

3.2. Tensile and creep tests

The tensile properties of the alloys are shown in Table 3. According to the results, the tensile properties of alloys exhibited a similar tendency at various temperatures. The ultimate tensile strength (UTS) and 0.2% offset yield strength (YS) increased with an increase in Re content up to a maximum of 3 wt%. The elongation (El) was nearly invariable in alloys containing 0–3 wt% Re; however, C(5Re) displayed the lowest of El.

Fig. 5 illustrates the typical strain-time creep curves of alloys under 871 °C/391 MPa conditions. The creep curves of each alloy

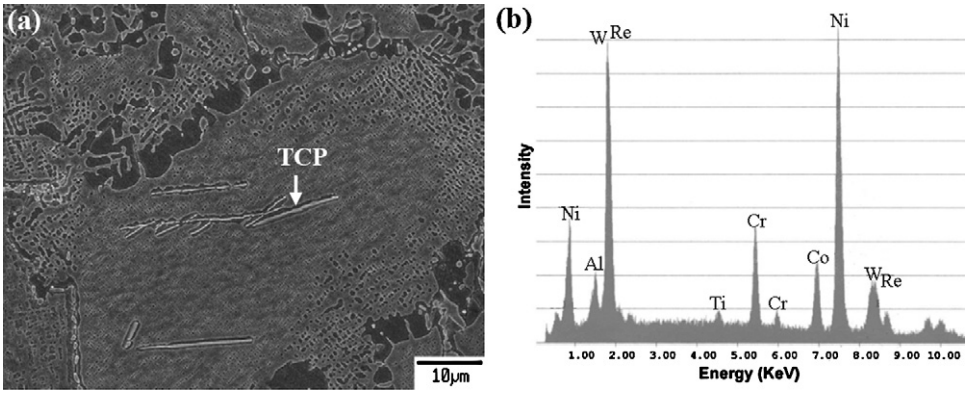

Fig. 2. (a) SEM microstructure of C(5Re) after heat treatment and (b) the EDS spectra of TCP phase.

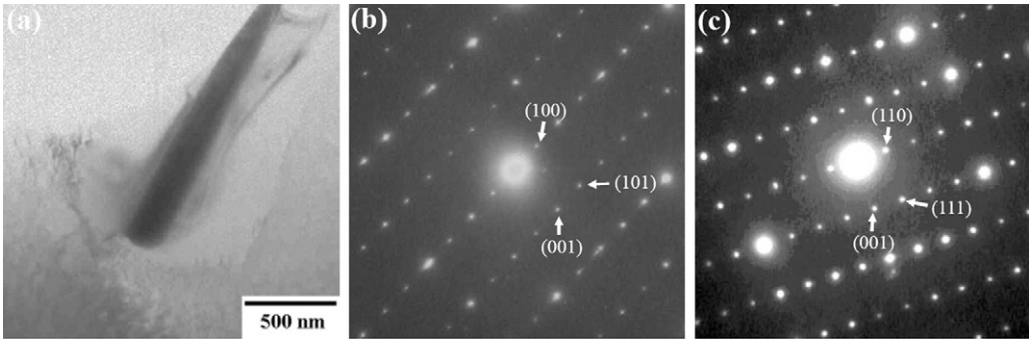

Fig. 3. The TEM (a) bright-field image of the P phase, (b) selected-area diffraction pattern (SADP) with [0 1 0] zone, and (c) [1 −1 0] zone.

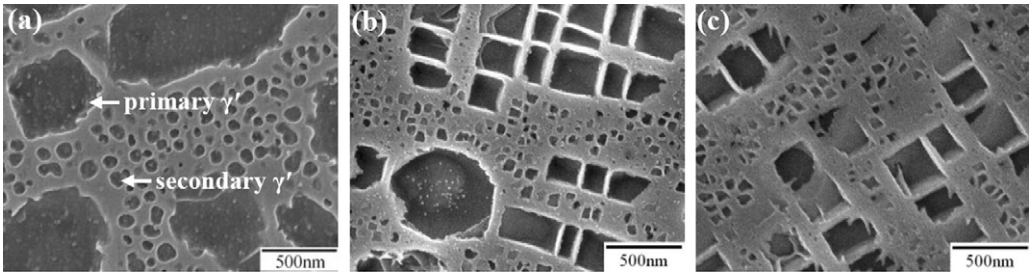

Fig. 4. The γ′ phase morphology of (a) Mar-M247, (b) B(3Re), and (c) C(5Re) after heat treatment.

Table 3
Tensile test results at various temperatures.

Temp.	Alloy	UTS (MPa)	YS (MPa)	El (%)
RT	Mar-M247	1121–1139	967–987	4.8–6.0
	A(1Re)	1124–1143	973–995	4.7–6.2
	B(3Re)	1190–1217	1043–1074	4.0–6.0
	C(5Re)	1083–1108	932–968	1.3–3.0
760 °C	Mar-M247	1146–1176	969–1013	4.4–6.0
	A(1Re)	1157–1183	985–1015	4.5–6.3
	B(3Re)	1228–1254	1066–1088	4.3–6.7
	C(5Re)	1071–1092	936–970	1.7–2.9
871 °C	Mar-M247	911–925	792–816	5.0–5.7
	A(1Re)	916–928	797–822	5.1–5.6
	B(3Re)	972–984	834–856	5.0–5.9
	C(5Re)	835–856	752–774	1.8–3.4

showed the same tendency, with a short primary creep stage, followed by a steady-state creep stage and then an accelerating (tertiary) creep stage leading to failure. Secondary creep rate or steady-state creep rate is one of the most important indications with regard to materials. A number of researchers believe that samples demonstrate a constant creep rate during the secondary creep and the life of this stage dominates nearly the entirety of creep life [12,13]. Other researchers have proposed that alloys have very short secondary creep regions with only one transient region of secondary creep, which can be considered the minimum creep rate [13,14]. They argue that the microstructure is not stable during high-temperature creep, resulting in the acceleration of the secondary creep rate leading to tertiary creep stage [13,14]. To better understand creep characters, the creep rate versus creep strain diagrams were produced, as shown in Fig. 6. One advantage of

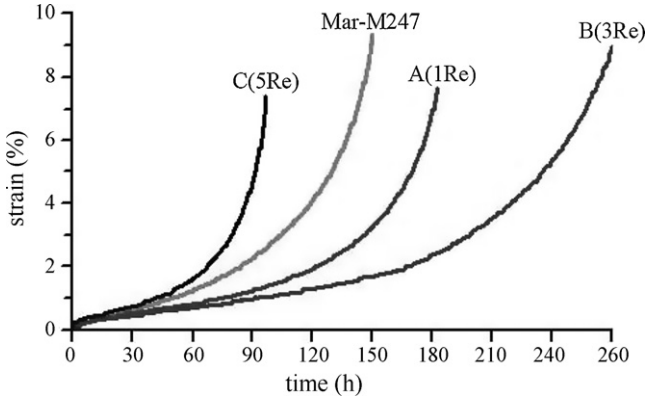

Fig. 5. Strain-time creep curves of Mar-M247 with various Re content tested under 871 °C/379 MPa.

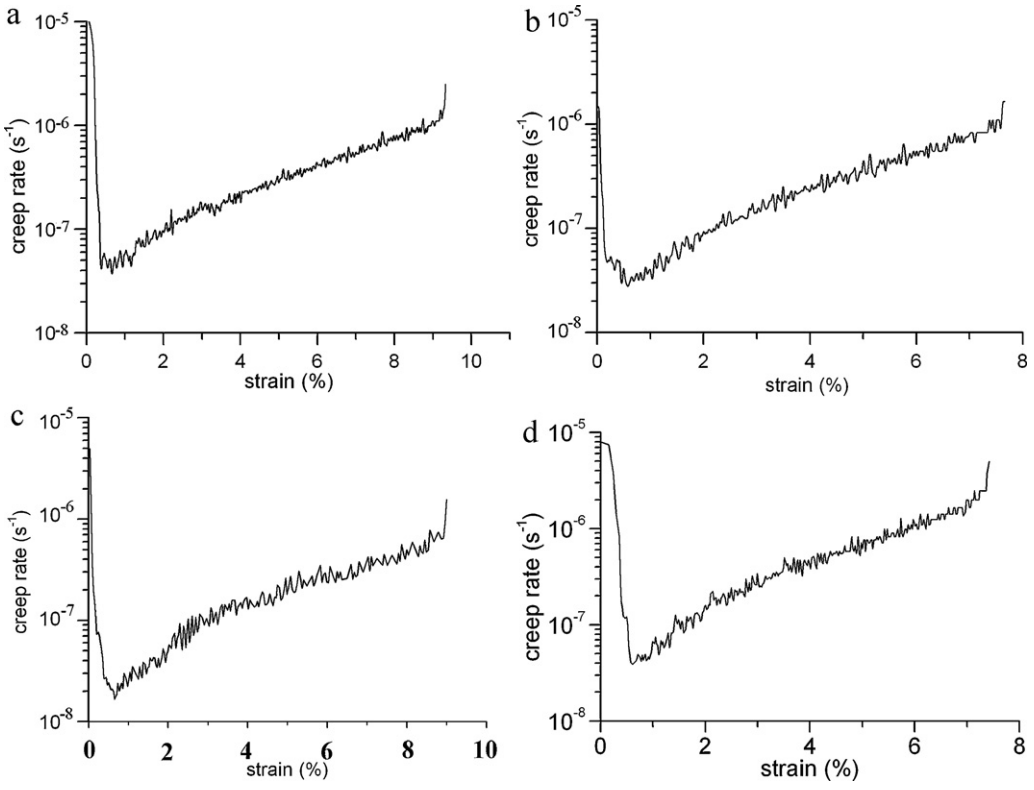

Fig. 6. Creep rate versus creep strain of (a) Mar-M247, (b) A(1Re), (c) B(3Re), and (d) C(5Re) under 871 °C/379 MPa (according to creep curve of Fig. 5).

Table 4
Creep test results of Mar-M247 with various Re content under 871 °C/379 MPa.

Alloy	Creep life (h)	El (%)	$t_{1\%}$ (h)[a]	$t_{2\%}$ (h)[a]	Min. creep rate (s^{-1})[a]
Mar-M247	149.3–184.4	9.3–10.5	49.3	83.6	3.8×10^{-8}
A(1Re)	168.9–213.3	7.3–10.1	80.5	116.6	2.7×10^{-8}
B(3Re)	260.0–296.6	7.1–9.1	90.3	166.5	1.6×10^{-8}
C(5Re)	96.4–143.5	6.4–8.1	41.3	67.1	3.9×10^{-8}
Mar-M247 (Grainex)[b]	217.9	7.6	77	124	–

[a] Obtained from creep diagrams of Fig. 6.
[b] Creep data of Grainex casting Mar-M247 are according to Ref. [5].

this method of presentation is that the regimes of increasing and decreasing creep strain rate can be easily identified. The creep diagrams of each alloy showed the same tendency. At first, the creep strain rate decreases with an increase in creep strain eventually reaching a minimum, implying that a creep hardening mechanism is active. Thereafter the creep rate increases with an increase in accumulated creep strain. It is clear that a minimum creep rate exists, rather than a steady-state condition. Table 4 summarizes the creep data. During service, turbine blades are usually strained below 1 or 2%, therefore the criterion of time to reach 1% ($t_{1\%}$) or 2% strain ($t_{2\%}$) was selected as a main indication of creep strength [5,15]. According to the aerospace structural metals handbook, the creep life of Grainex casting Mar-M247 superalloy, under the heat treatment and HIP conditions used in this study, is 217.9 h and the El is 7.6% at 871 °C/379 MPa [5]. It must be considered that the Grainex, the first generation of fine-grain casting technique developed by Howmet Corporation, produced casting with a fine-grain size about 360 μm [3,10]. That grain size is larger than the grain size in this study. Therefore, the Re-free Mar-M247 used in this study exhibits lower creep life than that of the alloy in the handbook. As it is evident in Table 4 that an increase in Re content up to a maximum of 3 wt% results in a reduction in the minimum creep rate and prolongs the $t_{1\%}$, $t_{2\%}$, and creep life. However, the addition of excessive Re, such as C(5Re), produced an alloy with the worst creep properties.

3.3. Fractographic observation and microstructural evolution

Observation of the fracture surface of a tensile tested specimen of Mar-M247 (Fig. 7a), shows that cracks occurred mainly along GB. A similar fracture is shown in A(1Re) and B(3Re) with cracks observed along the GB. Observation of the fracture surface of C(5Re) showed a crack on the GB, and a secondary crack was observed within the grain interior (Fig. 7b). The secondary cracks were very similar in size to the P phase observed in Fig. 2a. No other phases in the microstructure had similar dimensions. Obviously, secondary cracks initiated and propagated along the P/γ interface.

In the creep tests, the fracture surface of Mar-M247 showed that cracks occurred mainly along the GB (Fig. 8a). Fig. 8b shows identical cracking along the GB, indicating a typical intergranular fracture. A similar fracture mode appeared in the A(1Re) and B(3Re). On the fracture surface of C(5Re), cracks were observed on the GB, and secondary cracks were observed within the grain interior (Fig. 8c). Similarly, in Fig. 8d, cracks were observed along the GB and P/γ interfaces. The dimensions of needle-like P phase were similar to those of the secondary cracks observed in Fig. 8c. Obviously, the formation of P phases in C(5Re) provided another source for cracking.

Fig. 9a–c show the γ′ raft microstructure in samples of creep failure. Compared to as-heated microstructures, the obvious difference is the secondary γ′ phase directionally coarsened into rafts in the direction perpendicular to the stress axis. The morphology of primary γ′ phases appears not to be influenced by creep. Quantitative statistical analysis of the linear fraction of γ′ rafts in stress axial direction was determined according to micrographs of γ′ rafting. The statistical results show that the linear fraction of γ′ rafts increases with Re content up to a maximum of 3 wt%, from 36% to 48%, and then drops to 42%. To investigate the evolution of γ′ precipitates, creep tests of B(3Re) were interrupted in the primary and secondary creep stages, as shown in Fig. 9d and e, respectively. The interrupted samples show that secondary γ′ particles slightly coarsened into rafts in the primary creep stage and had already completed in the secondary creep stage. No substantial change in the rafted structure occurred as deformation proceeded.

4. Discussion

4.1. Correlation between microstructure and tensile properties

The strength of Ni-base superalloys at high temperature is attributed mostly to the characteristics of the γ′ precipitates and the strength of the γ matrix. Due to the primary γ′ with larger size, the primary γ′ has larger resistant than secondary γ′ to inhibit the movement of dislocation. Moreover, the quantities of the primary γ′ phase are much more than that of secondary γ′. Therefore, the primary γ′ played a more important role than the secondary γ′ as a determinant of strength. It has been reported that the YS is inversely related to the size of the primary γ′ in superalloys with a high volume fraction of γ′ [16]. Thus, the size of the primary γ′ phase decreased with an increase in Re content resulting in benefit to YS.

In addition, the strength of the γ matrix is another factor influencing YS and UTS. Studies have reported that the large atomic radius of Re partitioned mainly to the γ matrix resulting in the increase of the γ/γ′ lattice misfit and the strength of the γ matrix [17,18]. Durst used nanoindenting atomic force microscope to test the hardness of γ matrix in Re-containing superalloys, supporting the view described above [19]. In that research, it was shown an increase in the hardness of the γ matrix resulting from a higher concentration of Re. Additionally, fractographic analysis shows that adding excessive quantities of Re, such as C(5Re), provides an additional source of cracks. Moreover, the formation of P phases results in a decrease in solution-strengthening metal content (e.g. W, Re, Cr, and Co) within the γ matrix.

In summary, increased strength of the γ matrix and decrease size of primary γ′ resulting from the addition of Re, contributes to the improvement of YS and UTS. Conversely, a decrease in the quantity of γ′ and the formation of the needle-shaped P phase detracts from the strength. Therefore, we determined that an optimal Re content of 3 wt% provided optimal tensile properties between these conflicting factors.

4.2. Effects of microstructure and its evolution on creep behavior

According to the creep deformation map of a Mar-M247 related superalloy (Mar-M200), the creep mechanism with 100 mm grain size under the conditions of 871 °C/391 MPa was controlled by dislocation glide and climb [20]. When the γ′ particles are very small, it is easy for dislocations to cut or climb around them. Because the secondary γ′ is too small to efficiently resist dislocations and its quantities are much less than primary γ′, the primary γ′ played a more important role than the secondary γ′ as a determinant of creep strength. The dislocation glide is controlled by the strength of γ matrix and the inter-particle spacing in accordance with Orowan dislocation bypass model [21]. First, most studies have reported the presence of Re partitions with a large atomic radius in the γ matrix, increasing the strength of the γ matrix, thereby hindering movement of dislocations [17–19]. Second, this study verified that the inter-particle spacing between primary γ′ phases decreases with an increase in Re content up to a minimum of 3 wt%. In the early creep stage, microstructural evolution is not obvious. Therefore, a decrease in minimum creep rate with Re content up to 3 wt%, suggests that the addition of optimal quantities of Re could improve creep resistance by two ways: (1) increasing the strength of the γ matrix and (2) decreasing the inter-particle spacing.

In the later creep stage, the evolution of γ′ morphology is another major factor determining creep behavior. The γ′ raft impedes moving dislocations by eliminating the number of vertical (parallel to the direction of stress) γ channels. Once the rafted microstructure has formed, the Orowan effect does not have a direct influence on creep resistance. Two possibilities for the creep

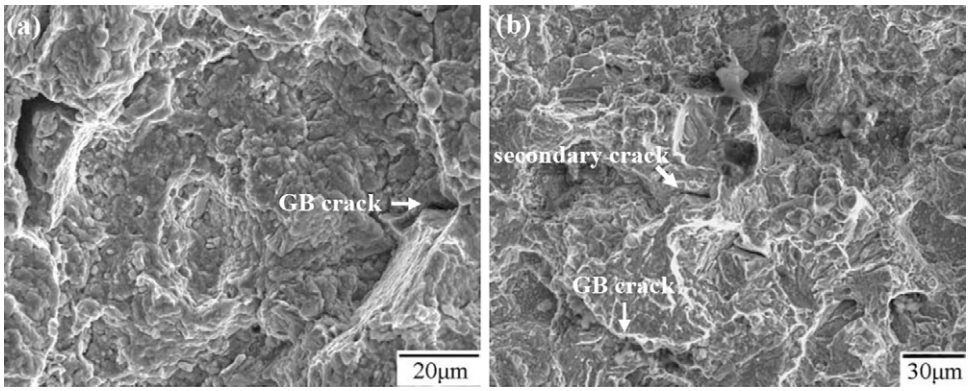

Fig. 7. Fracture surfaces of tensile test: (a) Mar-M247 and (b) C(5Re).

mechanism in the rafting regime can be envisaged: (1) dislocations shear the γ′ raft leading to further deformation; and (2) dislocations climb through the γ′ raft and continue deformation. These two factors are highly related to the strength and the number of γ′ rafts. Most previous studies have shown that Re partitions less strongly to the γ′ phase with no appreciable effect on the strength of the γ′ phase [17–19]. Therefore, changes in creep strength among various Re-containing alloys are not likely the result of invariant strengths of the γ′ phase. On the other hand, dislocations usually move in the direction parallel to the stress axis due to deformation in this direction. Thus, creep resistance is concerned mainly with the linear fraction of the γ′ raft in stress axial direction. Statistical results show that the linear fraction of the γ′ raft increases with Re content to a maximum of 3 wt%, and then drops. The increased linear fraction of γ′ rafts represents an increased likelihood that γ′ rafts will impede dislocations moving axially to the direction of the stress, resulting in the increased resistance. Therefore, alloys with a higher linear fraction in the γ′ raft, such as B(3Re), more effectively resist the movement of dislocations. It must be emphasized that the primary γ′ phases do not coarsen into rafts during creep. Primary γ′ particles still act as obstacles for moving dislocations. Therefore, creep resistance is not only relative to γ′ rafts but also relative to the primary γ′ phase. Interestingly, until now, most studies have discussed creep behavior on γ′ rafts which directionally coarsen from primary γ′ phases [22,23]. Few studies have investigated the role of γ′ rafts, directionally coarsened from the secondary γ′ phase, on creep behavior. That is because most studies discovered that the secondary γ′ dissolves during high-temperature creep [22,23].

Fractographic observations show that for C(5Re), the cracks propagated along the GB and the P/γ interface—adding another source for cracking. The needle-like P phase acts as a barrier for moving dislocations. Dislocations accumulated easily along the P/γ

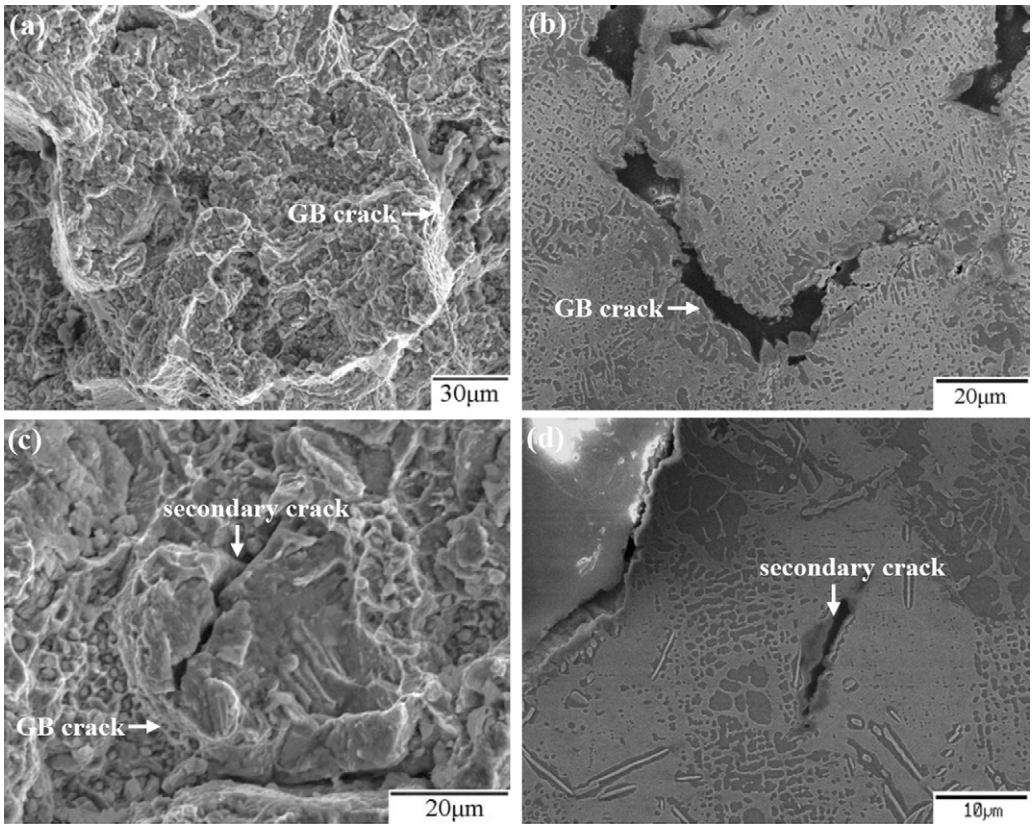

Fig. 8. Fractographs after creep test: (a) fracture surface and (b) longitudinal section of Mar-M247; (c) fracture surface and (d) longitudinal section of C(5Re).

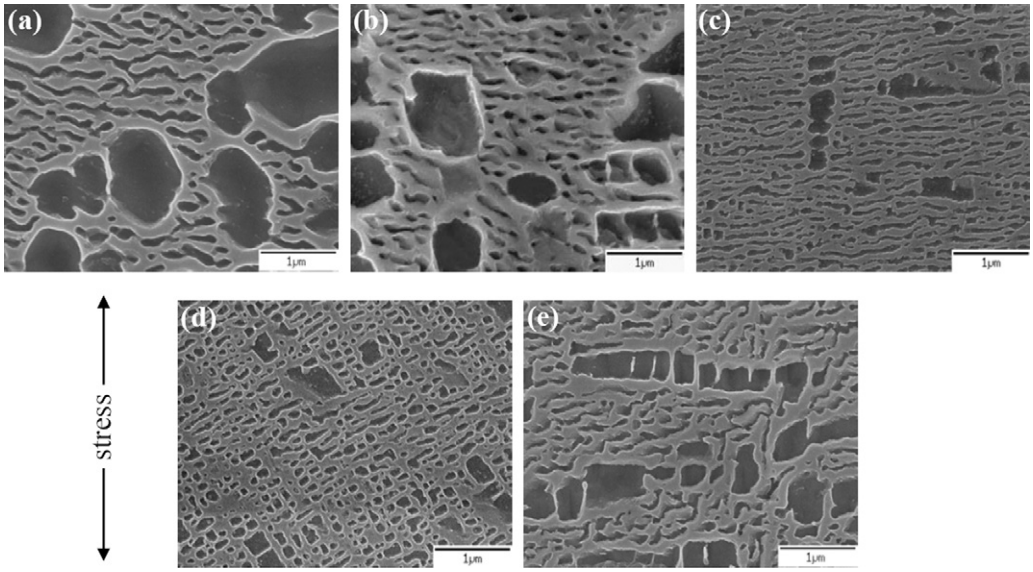

Fig. 9. Postcrept γ′ rafting microstructure of (a) Mar-M247, (b) B(3Re), and (c) C(5Re); γ′ evolution of B(3Re) after (d) 0.5% (in primary creep stage) and (e) 1.5% creep strain (in secondary creep stage). The applied tensile stress is in the vertical direction.

interface, leading to incoherence, and causing the appearance of interfacial cracking. Moreover, once cracks occur along the P/γ interface, they act as stress concentration sites and they also cause a decrease in the load-bearing cross-section, resulting in accelerated creep rate to failure. In addition, the formation of P phase removes the solid solution strengthening elements from the γ matrix resulting in a decrease in creep resistance. Therefore, the presence of the P phase is major factor detracting from creep strength.

To summarize, the influence of microstructure and its evolution on creep behavior in experimental alloys is governed by a number of interdependent microstructural parameters. In the early creep stage, the addition of Re increases the strength of the γ matrix and shortens the inter-particle spacing with a benefit to creep strength. The secondary γ′ phases directionally coarsening into γ′ rafts is the most obvious microstructural evolution during creep. In the later creep stage, the linear fraction of the γ′ raft increases with the addition of Re resulting in improved creep resistant. Finally, the addition of excessive Re, such as C(5Re), is detrimental to the creep properties due to the formation of the P phase. In this study, the optimal modified Mar-M247 superalloy with the best creep properties was B(3Re). According to Table 4, although the grain size of B(3Re) is finer than that of the Grainex casting Mar-M247, the creep properties of B(3Re) are superior to those of Grainex casting Mar-M247. This proves that the fine-grain casting of B(3Re) exhibits excellently creep properties at 871 °C. Therefore, the addition of 3 wt% Re Mar-M247 is a viable approach to producing a fine-grain superalloy with high creep resistance at high-temperatures.

5. Conclusions

In this study, we modified alloys through the addition of the element Re to Mar-M247. The base and modified alloys underwent tensile and 871 °C/379 MPa creep tests. Microstructure and its evolution and mechanical behavior were investigated. Conclusions could be summarized as follows:

1. Dual precipitation of γ′ particles including primary and secondary γ′ occurs in Mar-M247 and modified Mar-M247 superalloy. As the Re content increases, the primary γ′ phase becomes finer and reduces in abundance. The addition of Re does not have an obvious influence the secondary γ′ phase.
2. The tensile tests show that both UTS and YS increase with an increase in Re content up to a maximum of 3 wt%. The improvement in tensile properties results from the refinement of primary γ′ and improved strength in the γ matrix.
3. The secondary γ′ phase directionally coarsened into rafts in the direction perpendicular to the stress axis in a 871 °C/379 MPa creep test. However, the morphology of the primary γ′ phase was not influenced by creep. Interrupted creep tests verify that the γ′ rafting structure initiated in the primary creep stage and finished in the secondary creep stage, with no substantial change in the rafted structure occurring as deformation proceeds.
4. The 871 °C/379 MPa creep tests show that an increase in Re content up to a maximum of 3 wt% results in a reduction in minimum creep rate and prolongation of creep life. The addition of Re could improve creep resistance in the early creep stages by (1) increasing the strength of the γ matrix and (2) decreasing the inter-particle spacing. In the later creep stages, the linear fraction of γ′ rafts in stress axial direction increases with Re content to a maximum of 3 wt% contributing to an improvement in creep strength.
5. In tensile and creep tests, cracks initiated and propagated along the GB in Mar-M247 with 0–3 wt% Re. The addition of excessive Re, such as 5 wt%, resulted in the initiation and propagation of cracks along both the GB and P/γ interface, damaging both tensile and creep properties.

Acknowledgments

The authors would like to thank Mr. Y. P. Huang for his help in mechanical property evaluation. The equipment support of processing from Mr. J.S. Chen is also thankfully acknowledged.

References

[1] C.T. Sims, N.S. Stoloff, W.C. Hagel, Superalloys II, John Wiley & Sons, New York, 1987, pp. 420–426.
[2] C.N. Wei, H.Y. Bor, L. Chang, Mater. Sci. Eng. A 527 (2010) 3741–3747.
[3] L. Liu, T. Huang, Y. Xiong, A. Yang, Z. Zhao, R. Zhang, J. Li, Mater. Sci. Eng. A 394 (2005) 1–8.
[4] Allied-Signal Aerospace Company, Garrett Engine Division, 1991, Specification No. EMS52508.
[5] W.F. Brown, S.J. Setlak, Aerospace structural Metals Handbook, vol. 6, 39th ed., 1999, Code 4218.
[6] C.M.F. Rae, R.C. Reed, Acta Mater. 49 (2001) 4113–4125.

[7] S. Tin, T.M. Pollock, Mater. Sci. Eng. A 348 (2003) 111–121.
[8] C.T. Sims, N.S. Stoloff, W.C. Hagel, Superalloys II, John Wiley & Sons, New York, 1987, pp. 221-226.
[9] A. Volek, R.F. Singer, R. Buergel, J. Grossmann, Y. Wang, Metall. Trans. A 37A (2006) 405–410.
[10] L. Liu, T. Huang, Y. Xiong, A. Yang, Z. Zhao, R. Zhang, J. Li, Superalloys, TMS, Warrendale, PA, 2004, pp. 493–500.
[11] Y. Ma, J. Sun, X. Xie, Y. Hu, J. Zhao, P. Yan, J. Mater. Process. Technol. 137 (2003) 35–39.
[12] A.C. Yeh, A. Sato, T. Kobayashi, H. Harada, Mater. Sci. Eng. A 490 (2008) 445–451.
[13] J. Safari, S. Nategh, Mater. Sci. Eng. A 499 (2009) 445–453.
[14] R.C. Reed, N. Matan, D.C. Cox, M.A. Rist, C.M.F. Rae, Acta Mater. 47 (1999) 3367–3381.
[15] M.V. Acharya, G.E. Fuchs, Mater. Sci. Eng. A 381 (2004) 143–153.
[16] C.T. Sims, N.S. Stoloff, W.C. Hagel, Superalloys II, John Wiley & Sons, New York, 1987, pp. 206.
[17] J. Rüusing, N. Wanderka, U. Czubayko, V. Naundorf, D. Mukherji, J. Rösler, Scripta Mater. 46 (2002) 235–240.
[18] P.J. Warren, A. Cerezo, G.D.w. Smith, Mater. Sci. Eng. A 250 (1998) 88–92.
[19] K. Durst, M. Göken, Sci. Eng. A 387-389 (2004) 312–316.
[20] C.T. Sims, N.S. Stoloff, W.C. Hagel, Superalloys II, John Wiley & Sons, New York, 1987, pp. 40.
[21] C.T. Sims, N.S. Stoloff, W.C. Hagel, Superalloys II, John Wiley & Sons, New York, 1987, pp. 77-78.
[22] R.C. Reed, N. Matan, D.C. Cox, M.A. Rist, C.M.F. Rae, Acta Mater. 47 (12) (1999) 3367–3381.
[23] R.C. Reed, D.C. Cox, C.M.F. Rae, Mater. Sci. Eng. A 448 (2007) 88–96.